Integrated Communications and Non-Invasive Vibrations Sensing using Strobing Light

Muhammad Sohaib Amjad and Falko Dressler
Heinz Nixdorf Institute and Dept. of Computer Science, Paderborn University, Germany
{amjad,dressler}@ccs-labs.org

***Abstract*—Vision-based techniques for advanced monitoring of industrial systems is gaining more attention recently. A good example is the use of cheap low frame rate cameras in combination with strobing light to non-intrusively measure high frequency vibrations. At the same time, we see an uprise of Visible Light Communication (VLC), particularly for indoor usage. In this paper, we bridge the gap between these two concepts and propose an integrated communication and sensing system based on strobing light. Our system can reproduce the same signal envelope while VLC is in operation, thus, hiding communication from the camera-based sensing. We explored the performance of the system using a GNU Radio implementation. Our results demonstrate the huge potentials of this integrated communication and sensing concept.**

I. Introduction

Vision-based monitoring of objects such as structures, machines, etc, for safety purposes, have gained significant attention [1]. Such monitoring is not only needed for the detection of anomalous behavior that can result in potential breakdowns, but also for the continuous optimization of the operating parameters (e.g., machinery in an industrial operation) for maximum performance throughput. These indicators can provide a comprehensive picture of a machine under inspection, which certainly helps during inspections to identify whether it is fully operational/functional/safe-to-use. If a deterioration is detected, it requires immediate attention and it should be replaced/resolved; any negligence can potentially lead to severe health and safety-risks.

In this regard, the analysis of vibrations is extensively used as the first indicator of possible faults/failures. The spectral analysis of vibration signals from an object, e.g., a machine with rotating parts, can provide useful insights into its mechanical conditions and working [2]. Classically, vibrations are typically measured using contact-based velocity or accelerometer sensors. However, such sensors are required to be mounted on the object under investigation, and thus poses operational and deployment challenges, especially in high-risk environments, such as high-temperature, high-pressure, or radioactive areas within a plant.

Contact-less approaches for measuring these vibrations have emerged as an attractive alternative, and they have been the focus many researchers since last decade. The Laser Doppler Vibrometer (LDV) [3] and Near-field Acoustic Holography (NAH) [4] are the two most precise contact-less vibration measurement devices. The vision-based estimation of vibrations via a high Frames Per Second (FPS) camera [5]–[7], has also emerged as a popular at-a-distance measuring approach. Recently, Roy et al. [2], [8] experimentally demonstrated an alternative vision-based technique, which utilizes a commodity low FPS camera to measure high-frequency vibrations using strobing light. The used optical strobing signal is a narrow width optical pulse with adjustable frequency. This strobing pulse optically samples the object/machine under observation, which effectively modulates the vibration signal, and shift the frequency components (by exploiting the frequency folding phenomenon) within the Nyquist frequency of the low FPS camera.

Besides the facilitation of optical signal in such non-invasive sensing applications, it has also demonstrated wireless communication capabilities [9]. Recent works, such as [10] have utilized intensity modulation and direct detection approach with LEDs and Photo-Detector (PD) to transmit data through the optical wireless channel over distances as far as 75 m. Apart from [10], a substantial amount of works, e.g., [11]–[13], have experimentally shown visible-light as a (less-expensive) potential candidate to complement the exiting radio-frequency based wireless communications.

The capacity of an optical signal to perform both sensing and communications can be exploited in an integrated fashion to mutually benefit from each other, i.e., utilizing the same optical sensing signal for communications as well. In this paper, we bridge this gap between the two domains, and propose an integrated system for simultaneous communications and non-invasive sensing of an object's vibrations. We implement the communication part which uses BPSK modulation and supports a data rate of 80 kB/s, and emulate the sensing part to detect the frequencies with and without the communication signal jointly in the GNU Radio framework.

Our main contributions can be summarized as follows:

- For the first time, we present and investigate an integrated system for simultaneous communications and non-invasive sensing for potential fault/failure detection;
- we investigate the impact of the sensing signal on the communications performance, and demonstrate that the performance drop is close to 0.5 dB only;
- we study the error in the envelope of the resulting strobing signal, i.e., with and without the communication signal, and show that the error is below −50 dB; and
- we analyze the detected frequencies of the strobing signal, and establish that the absolute error is below −65 dB.

II. Related Work

Contact-based velocity and accelerometer senors are often the first choice for the vibration measurement of an object, e.g., structures and machinery. However, these sensors not only poses deployment and operational challenges in high-risk locations, but also result in additional time and expenses for the collection of measurement data. Contact-less vibration sensing approaches such as LDV [3] and NAH [4], either measure the pressure readings of the vibrating surface or utilize a group of highly synchronized lasers for the frequency estimation. Although these approaches offer precise vibration frequency estimates, the equipment is rather expensive, and the estimation time increases with the size of the object.

Recently, vision-based vibration estimation techniques have emerged as an attractive at-a-distance measuring alternatives [5], [7]. These contract-less approaches perform image processing on a series of frames captured by a camera, and provide compelling vibration frequency estimates. Nevertheless, to measure high-frequency vibrations precisely, specialized/expensive high FPS cameras are required to avoid aliasing problem. The high-frequency vibrations through a low FPS camera have been experimentally measured by exploiting optical strobing phenomenon [2]. In this work, a strobing signal has been used with adjustable frequency to optically samples the object under observation, which effectively modulates the vibration signal, and shift the frequency components within the Nyquist frequency of the low FPS camera.

At the same time, optical signals have been shown to have the potential of wireless communications as well. For example, a GNU Radio-based Visible Light Communication (VLC) prototype for IEEE 802.15.7 standard has been introduced [11]. Similarly, in [12], a VLC-based infrastructure-to-vehicle communication prototype is presented, which can perform reliably up to 40 m distances. In [13], a white LED-based indoor broadband wireless system has been presented achieving a data rate of 1 Gbit/s. These studies demonstrated the potential of optical signal to complement the existing radio-frequency based wireless systems.

In this paper, we combine the two domains, i.e., the sensing and communications via optical signal, for mutual gain. We first study the impact of combining the communications and sensing signal mathematically, and then analyze the integration via real-time simulation experiments.

III. Optical Strobing for Sensing Applications

When a vibrating object is illuminated with some external periodically strobing light source, it results in a different presentation of the motion, i.e., the visual appearance of that object to a viewer changes. A frame-to-frame comparison of that illuminated object (via image processing tools) provides the temporal speed of the change in presentation. This temporal speed and object position information can be further utilized to estimate the unknown vibrational frequency of that object to a great precision [2]. By exploiting this optical strobing phenomenon to measure any changes in the vibrational frequency of an object, it becomes possible to unobtrusively detect system faults/failures. Such unobtrusive detection is especially beneficial in hazardous environments, where human intervention is least-desirable.

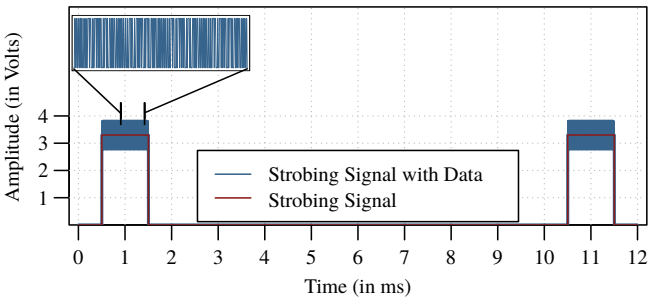

Figure 1. Optical strobing signals (with and without data) used for the performance comparison in the proposed integrated system.

A. Strobing Principle

The strobing signal is a narrow width periodic pulse [14] as illustrated in Figure 1. This signal is basically used to turn on an LED panel, which illuminates the object under observation periodically for short durations, i.e., the optical sampling. The optically sampled object $g_s(t)$ can be expressed mathematically as

$$g_s(t) = g(t) \times c(t), \tag{1}$$

where $g(t)$ is the object with unknown vibrational frequency, and $c(t)$ is the infinite strobing optical pulse train, i.e., $c(t) = \sum_{n=-\infty}^{\infty} \delta(t - nT_s)$, of known period T_s. The Fourier domain representation of Equation (1) can be written as

$$G_s(\omega) = \frac{1}{2\pi}[G(\omega) \circledast \frac{2\pi}{T_s} \sum_{k=-\infty}^{\infty} \delta(\omega - k\omega_s)], \tag{2}$$

where ω_s is the optical sampling frequency, and k is of integer nature. The optically sampled signal $G_s(\omega)$ is obtained as

$$G_s(\omega) = \frac{1}{T_s} \sum_{k=-\infty}^{\infty} G(\omega - k\omega_s). \tag{3}$$

The resulting sampled signal is captured by a low FPS camera with a frame rate ω_{cam} that effectively acts as a low-pass filter. The camera (aligned with the LED panel) sends the captured video of the object to a signal processing software (e.g., MATLAB). The software then performs a frame-to-frame analysis of the video for the extraction of temporal speed and position information, in order to estimate the vibrational frequency of that object.

B. Strobing Condition

Using the Nyquist sampling criterion, the condition of aliasing-free strobing can be defined as

$$2 \times |\omega - k \times \omega_s| \leq \omega_{\text{cam}}, \tag{4}$$

This condition certainly bounds the detectable vibrational frequency range with ω_{cam}, which, for a cheap low FPS camera, is already quite small. Nevertheless, we can deliberately alias

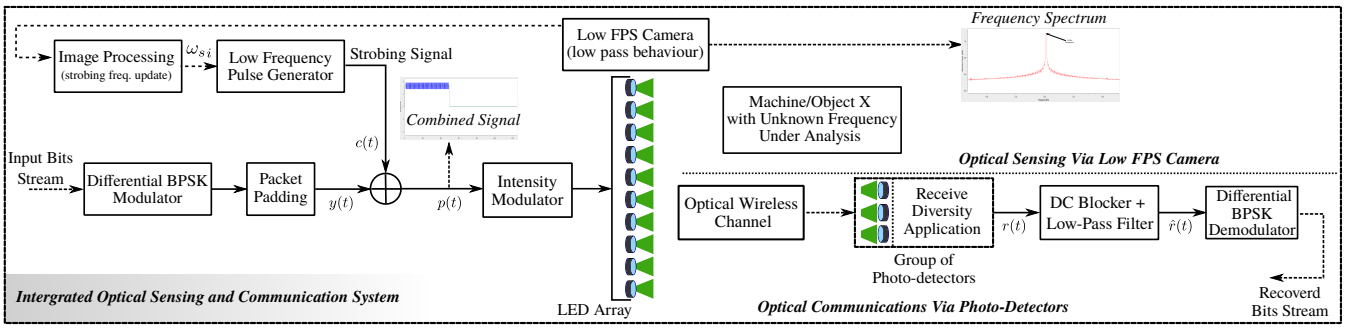

Figure 2. Block diagram of our integrated wireless system for simultaneous communications and non-invasive optical sensing.

the periodic signals by sampling them with a frequency that is very close to the fundamental frequency. The frequency folding phenomenon as a result of this intentional aliasing shifts the sampled periodic signal spectrum within the range of ω_{cam}. Thus, the aliased frequency will fall within the low-pass behavior of the camera ω_{cam} only, if the following condition is satisfied:

$$2 \times ||\omega - k \times \omega_s| - \omega_{\text{cam}}| \leq \omega_{\text{cam}}, \tag{5}$$

Hence, if k can be estimated, the unknown vibration frequency ω can be calculated.

C. Combined Strobing with Communications

For the combined communications and sensing, we add the communication signal with the strobing signal only during the *ON-Time* of the strobing pulse as shown in Figure 1. Since the sampling frequency for the communication signal is over ten thousand times higher than the strobing signal, it is expected to not to distort the optical sampling pulse. We study and demonstrate the impact of adding the communication signal on the strobing pulse and vice versa in the following, both mathematically and via simulation experiments.

IV. System Model

Figure 2 shows the detailed block diagram of our integrated system. In this section, we first model a free-space optical channel, and then mathematically study the integrated sensing and communication parts within the considered system.

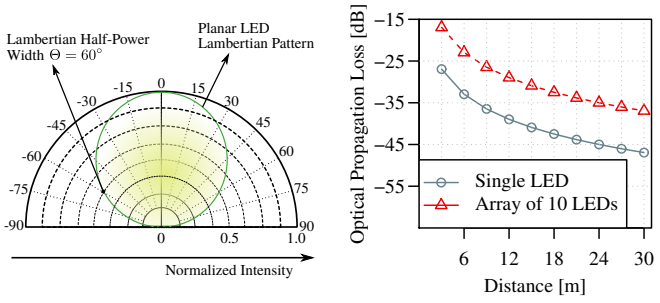

(a) Lambertian (LED) radiation pattern. (b) Optical propagation loss.

Figure 3. Optical propagation loss over increasing distances in the free-space for Lambertian pattern-based single LED and an array of 10 LEDs.

A. Optical Wireless Channel

The fundamental characteristics of the optical wireless channel highly depend on the optical link design, configuration, and topology [15]. Optical wireless systems are typically classified according to the degree of directionality between the optical transmitter and receiver, the existence of a continuous line-of-sight path, and the divergence angle of an optical transmitter and the field-of-view of an optical receiver. For such a classification, the propagation in an optical wireless channel can be expressed as

$$P_r = P_s \cdot G_{Tx} \cdot G_d \cdot G_{Rx} \cdot A_{losses}, \tag{6}$$

where P_r is the received signal strength, P_s is transmitted signal power, G_{Tx} is the optical transmitter gain, G_{Rx} is the optical receiver gain, G_d is the light intensity depreciation over distance, and A_{losses} are the system-dependent losses due to the design and configuration.

The optical transmitters, such as LEDs, are typically designed to have a spatial luminous intensity that follows Lambertian beam distribution (cf. Figure 3a). With a Lambertian beam under-filling the transmitting aperture and a typical PD for absorbing the light, the optical transmitter-receiver gains along with propagation loss [16] can be calculated as

$$G_{Tx} = \frac{32}{\Theta^2}; \quad G_{Rx} = \left(\frac{\pi D}{\lambda}\right)^2; \quad G_d = \left(\frac{\lambda}{4\pi \cdot d}\right)^2,$$

where Θ is the full-angle transmit beam divergence (in rad), D is the diameter of the optical receiver aperture, d is the distance between the optical transmitter-receiver system, and λ is the wavelength. After substitution of the values of the gains, Equation (6) can be written as

$$P_r = P_s \cdot \frac{2D^2}{\Theta^2 d^2} \cdot A_{losses}, \tag{7}$$

with free-space propagation loss (α) being computed as

$$\alpha = \frac{2D^2}{\Theta^2 d^2} \cdot A_{losses}, \tag{8}$$

In Equation (8), it can be seen that, besides the distance between transmitter and receiver, the attenuation coefficient α also depends on the transmitter beamwidth and the receiver's aperture diameter. A wider beam divergence further increases the α, and a larger aperture reduces the attenuation coefficient as it can absorb more light.

The far-field pattern generated by an LED defines its maximum intensity region. Typical LEDs with Lambertian pattern (cf. Figure 3a) have an angular intensity distribution which is maximum near $0°$, and reduces to 50% at an angle of $60°$, thus, having a theoretical half-power beamwidth at $\Theta = 120°$. An LED with such divergence angle for transmissions and an optical receiver/detector with an aperture diameter of 0.3 m, the free-space optical propagation loss over distance is obtained as shown in Figure 3b. The propagation loss shown in the plot does not include system-dependent losses A_{losses}. These propagation loss values over distance are later used in Section V-C to model the free-space optical channel for simulative evaluation purposes.

B. Optical Communication Model

For the optical wireless communication part (cf. Figure 2), the bit-stream to be sent is differentially BPSK modulated first, and then combined with the sensing signal to obtain the resultant signal as

$$p(t) = y(t) + c(t), \tag{9}$$

where $y(t)$ is the communication signal, and $c(t)$ is the periodic strobing pulse generated to perform the optical sampling for sensing via low FPS camera. This combined signal $p(t)$ is then intensity-modulated onto an array of 10 LEDs for optical transmission. For the case of a single optical receiver, i.e., the PD, the received electrical signal $r(t)$ is obtained as

$$r(t) = A + \alpha p(t) + n(t), \tag{10}$$

where A is the DC offset added by the intensity modulator, α is the attenuation coefficient due to optical propagation loss, and $n(t)$ is the zero mean Additive White Gaussian Noise (AWGN). Since the communication signal $y(t)$ is added on top of the constant strobing signal $c(t)$, the signal after the DC blocker and filtering ($\hat{r}(t)$) can be written as

$$\hat{r}(t) = \alpha\hat{y}(t) + n(t). \tag{11}$$

Following the low-pass filtering, the received differential BPSK signal is demodulated and decoded to recover the bit-stream.

The obtained instantaneous received Signal-to-Noise Ratio (SNR) γ_{rx} of the overall integrated system is calculated as

$$\gamma_{rx} = \frac{\alpha^2 \cdot P_s}{\sigma^2}, \tag{12}$$

where $E\{|\hat{y}(t)|^2\} = P_s$ is the instantaneous signal power and $E\{|n(t)|^2\} = \sigma^2$ is the noise power.

C. Optical Sensing Model

By employing the combined strobing signal, as illustrated in Figure 1, the optically sampled object ($g'_s(t)$) can be mathematically expressed as

$$g'_s(t) = g(t) \times (y(t) + c(t)). \tag{13}$$

The Fourier domain representation of (13) is obtained as

$$G'_s(\omega) = \frac{1}{2\pi}[G(\omega) \circledast Y(\omega) + G(\omega) \circledast C(\omega)], \tag{14}$$

where $G(\omega)$ is the object with unknown frequency, and $C(\omega)$ is the periodic strobing pulse train, i.e., $C(\omega) = \frac{2\pi}{T_s}\sum_{k=-\infty}^{\infty}\delta(\omega - k\omega_s)$. The resultant optically sampled signal can be written as

$$G'_s(\omega) = \frac{1}{T_s}\sum_{k=-\infty}^{\infty} G(\omega - k\omega_s) + \frac{1}{2\pi}[G(\omega) \circledast Y(\omega)]. \tag{15}$$

The sampled signal in Equation (15) is captured by a low FPS camera. The low-pass behavior of the camera filter outs the high frequency communication signal, and the residual signal is obtained as

$$G'_s(\omega) = \frac{1}{T_s}\sum_{k=-\infty}^{\infty} G(\omega - k\omega_s) + N(\omega), \tag{16}$$

where $N(\omega)$ is the filtered noise. The resulting error in the sampled object due to the two different strobing signals is computed by subtracting (3) from (16) as

$$||e_{err}||^2 = ||G'_s(\omega) - G_s(\omega)||^2 = ||N(\omega)||^2. \tag{17}$$

From Equation (17), it can be seen that when $N(\omega) \to 0$, the two strobing signals samples the object in a similar fashion.

V. Performance Evaluation

A. Implementation Details

To evaluate the proposed system with combined sensing and communication, we implemented the communication part and emulated the sensing part in the GNU Radio[1] framework. GNU Radio is widely used as a real-time signal processing framework supporting both simulations as well as Software Defined Radio (SDR)-based experiments, and is particularly suited for rapid prototyping. The graphical GNU Radio Companion (GRC) allows to monitor received/processed samples in real-time in both time and frequency domains. The GNU Radio-based implementation of our proposed integrated system comprises of two parts:

(1) Communications – We implemented differential BPSK modulation/demodulation to modulate the bit-stream. A low-pass filter following the DC blocker is added at the receiving end before demodulation, to block the DC component due to the strobing signal $c(t)$ and the corresponding high-pass behavior. Additionally, we used the model for propagation losses in an optical channel (cf. Section IV-A) with an LED array panel of size 10×1 as the transmitter, and the basic AWGN, to model the Photo-Detector noise.

(2) Sensing – To study the impact of adding the communication signal $y(t)$ on the strobing signal $c(t)$ for optical sensing, we first calculated the difference in the envelopes of the two simulated signals, i.e., with and without communication signal (cf. Figure 1), as

$$||\text{Err}||^2 = ||\text{Envelop} < c(t) > - \text{ Envelop} < p(t) > ||^2. \tag{18}$$

Figure 4 shows the error magnitude due to the difference in the envelopes of the two signals. It can be seen that the mean error

[1] https://www.gnuradio.org/

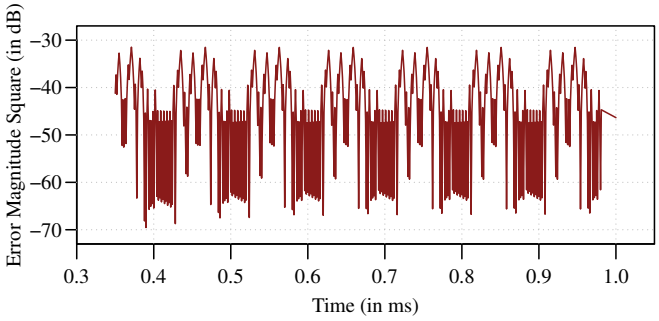

Figure 4. Magnitude of error between the envelopes of the two strobing signal, i.e., with and without the communication signal.

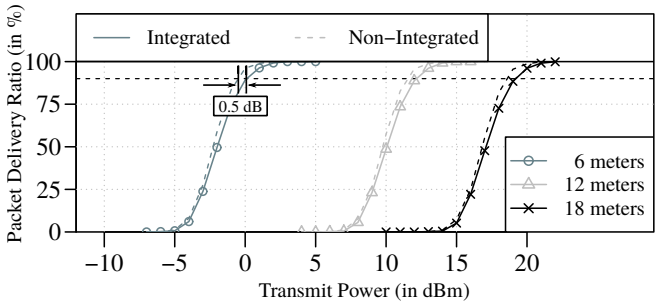

Figure 5. Measured Packet Delivery Ratio (PDR) with a single Photo-Detector (PD) for different distances and increasing transmit power levels.

is below −50 dB, which is extremely small. This minuscule impact of adding the communication signal on the sensing signal certainly ensured the possibility of combining both, i.e., sensing and communications.

In the second step, we emulated the low-pass behavior of a low FPS camera within GNU Radio and measured some known frequencies of strobing pulses with and without the communications signal.

B. Measurement Setup

For the performance evaluation of the proposed combined sensing and communication system, we conducted extensive real-time simulation experiments. We investigated the Packet Delivery Ratio (PDR) performance for the communications part in an optical wireless propagation scenario, and the test-frequencies detection for the sensing part by emulating a low FPS camera behavior.

In our simulation setup, we transmitted 100 differentially BPSK modulated packets during the *ON-Time* of the sampling pulse. Each sampling pulse carries 80 B of data, including a 2 B preamble, 1 B start-of-frame, and 1 B CRC. The transmission of packets is repeated 10 times to obtain a 95 % confidence interval, which for the sake of clarity, is not shown in the plots. The most relevant simulation parameters are listed in Table I.

C. Optical Communications Performance

1) Single Detector: Figure 5 shows the PDR performance with a single PD over increasing transmit power levels and for different distances. The horizontal dashed line marks 90 % PDR, with 100 % indicating that all the packets have been correctly detected and decoded. Also, the continuous line-plot

Table I
KEY PARAMETERS OF COMBINED SENSING & COMMUNICATION SYSTEM.

Modulation	Differential BPSK
Photo-Detector Aperture	0.3 m
LED Array	10×1
Packets Sent	100
Bytes-per-Pulse	80 B
Sampling Frequency	2 MHz
Optical Pulse Frequency	100 Hz
Emulated Low FPS Camera Cut-off	100 Hz
Noise Floor	−54 dBm (14-bit DAC)

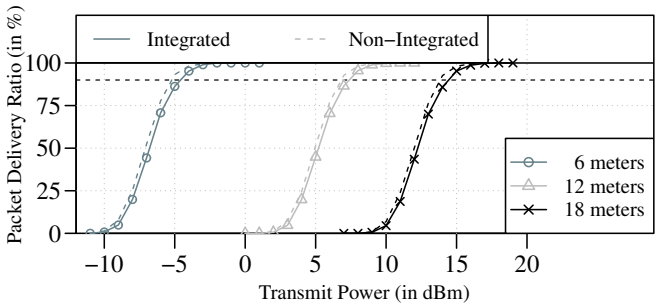

Figure 6. Measured Packet Delivery Ratio (PDR) with three Photo-Detectors (PDs) employing EGC diversity combining. The PDR is computed with increasing transmit power levels over multiple distances.

demonstrates the PDR performance with the integrated system, i.e., combined sensing and communications. Whereas, the dashed line non-integrated plots present the PDR performance without the sensing signal. Clearly, the addition of a sensing signal does have an impact on the PDR performance, which is dropped down by approx. 0.5 dB in-case of the integrated system. This performance drop is certainly because of the high-pass behavior of the DC blocker. Nevertheless, given the gains of the integrated system, this small performance degradation is inconsequential.

2) Multiple Detector: Figure 6 presents the PDR performance with a group of three PDs, where receive-diversity is applied to combine the signal received at each detector via the Equal Gain Combining (EGC) technique. As the detectors are right next to each other and absorb roughly similar light intensity [17], a simple micro-diversity approach with co-phasing of the received signal at each detector, is used to accomplishes EGC diversity. From the PDR comparison in Figures 5 and 6, a performance gain of close to 4.5 dB is measured with the three PDs over a single PD. A similar performance gain is also reported for three branch diversity in [18]. The deployment of multiple detectors can certainly improve the performance of the overall system without additional cost and hardware.

D. Frequency Sensing during Communication

To gain some insights on the impact of communication signal on the sensing pulse, we sampled some known low frequencies (10 Hz and 70 Hz) with both types of strobing signals, i.e., integrated and non-integrated systems. As can be

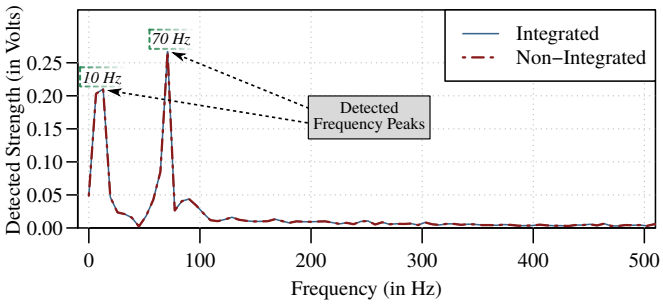

Figure 7. Detected low frequencies with the integrated pulse, i.e., combined sensing and communication signal.

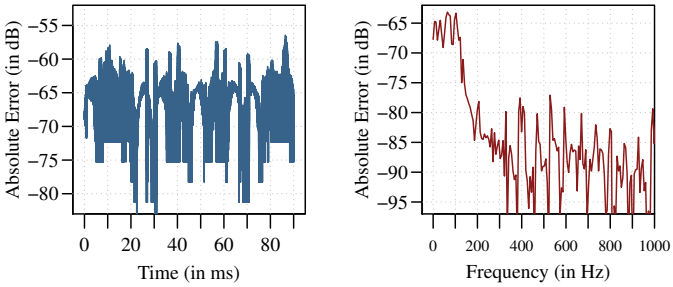

(a) Time domain. (b) Frequency domain.

Figure 8. Absolute error in the detected frequencies due to the integrated and non-integrated strobing pulses in the emulated sensing environment.

seen in Figure 7, the frequency detection results are remarkably similar with both strobing signals. Such close frequency detection results are rather expected as we have already seen a quite small error magnitude between the envelopes of two pulse in the earlier section (cf. Figure 4).

In Figure 8, we further present the absolute error in the detected frequencies (10 Hz and 70 Hz) due to the two types of strobing signals in both time-domain Figure 8a and frequency-domain Figure 8b. In both domains, the absolute error is close to −65 dB, which is microscopic and agrees with the absolute error between the envelopes of the two signals. Additionally, the low pass behavior in the frequency-domain (Figure 8b), is because of the emulated behavior of the camera. These results clearly indicate that combining the sensing and communication signal does not introduce any considerable error while sensing and, thus, support the proposed idea of integrating the two systems for mutual advantage.

VI. Conclusion

We presented a novel integrated wireless system for simultaneous communications and non-invasive sensing for the vibration measurements of an object. Our system, for the first time, bridged the gap between the two domains. Using simulations, we showed that the Packet Delivery Ratio (PDR) performance of the proposed system only drops by 0.5 dB, when combined with the strobing signal, for a distance of 6 m–30 m. We also demonstrated that the error between the envelopes of the sensing signals in integrated and non-integrated modes is below −50 dB, and the resultant error in the sensed frequencies is below −65 dB. Our results have shown that combining the sensing and communications signal only incurs a small drop in the performance. Such an integrated system can be deployed in remote locations such as high-temperature/pressure or radioactive areas, where the communications part can be used to send the sensed data wirelessly.

References

[1] A. M. Wahbeh, J. P. Caffrey, and S. F. Masri, "A vision-based approach for the direct measurement of displacements in vibrating systems," *Smart materials and structures*, vol. 12, no. 5, p. 785, 2003.

[2] D. Roy, A. Ghose, T. Chakravarty, S. Mukherjee, A. Pal, and A. Misra, "Analysing Multi-Point Multi-Frequency Machine Vibrations using Optical Sampling," in *IoPARTS 2018*, Munich, Germany, Jun. 2018, pp. 55–59.

[3] P. Castellini, M. Martarelli, and E. Tomasini, "Laser Doppler Vibrometry: Development of advanced solutions answering to technology's needs," *Elsevier, Laser Doppler Vibrometry*, pp. 1265–1285, 2006.

[4] M. Martarelli and G. Revel, "Laser Doppler vibrometry and near-field acoustic holography: Different approaches for surface velocity distribution measurements," *Mechanical systems and signal processing*, vol. 20, no. 6, pp. 1312–1321, 2006.

[5] J. G. Chen, N. Wadhwa, Y.-J. Cha, F. Durand, W. T. Freeman, and O. Buyukozturk, "Structural modal identification through high speed camera video: Motion magnification," in *IMAC 2012*. Brescia, Italy: Springer, Jul. 2012, pp. 191–197.

[6] P. McFadden and J. Smith, "Vibration monitoring of rolling element bearings by the high-frequency resonance technique—a review," *Tribology international*, vol. 17, no. 1, pp. 3–10, 1984.

[7] K.-S. Son, H.-S. Jeon, J.-H. Park, and J. W. Park, "A technique for measuring vibration displacement using camera image," *Transactions of the Korean Society for Noise and Vibration Engineering*, vol. 23, no. 9, pp. 789–796, 2013.

[8] D. Roy, S. Mukherjee, B. Bhowmik, A. Sinharay, R. Dasgupta, and A. Pal, "An autonomous, non-invesive vibration measurement system using stroboscope," in *ICST 2016*, Chinandega, Nicaragua, Nov. 2016, pp. 1–6.

[9] P. H. Pathak, X. Feng, P. Hu, and P. Mohapatra, "Visible Light Communication, Networking, and Sensing: A Survey, Potential and Challenges," *IEEE Communications Surveys & Tutorials*, vol. 17, no. 4, pp. 2047 – 2077, Feb. 2015.

[10] M. S. Amjad, C. Tebruegge, A. Memedi, S. Kruse, C. Kress, C. Scheytt, and F. Dressler, "An IEEE 802.11 Compliant SDR-based System for Vehicular Visible Light Communications," in *IEEE ICC 2019*. Shanghai, China: IEEE, May 2019.

[11] C. G. Gavrincea, J. Baranda, and P. Henarejos, "Rapid prototyping of standard-compliant visible light communications system," *IEEE Communications Magazine*, vol. 52, no. 7, pp. 80–87, Jul. 2014.

[12] N. Kumar, N. Lourenço, D. Terra, L. N. Alves, and R. L. Aguiar, "Visible Light Communications in Intelligent Transportation Systems," in *IEEE IV 2012*. Alcalá de Henares, Spain: IEEE, Jun. 2012.

[13] A. M. Khalid, G. Cossu, R. Corsini, P. Choudhury, and E. Ciaramella, "1-Gb/s Transmission Over a Phosphorescent White LED by Using Rate-Adaptive Discrete Multitone Modulation," *IEEE Photonics Journal*, vol. 4, no. 5, pp. 1465–1473, Oct. 2012.

[14] A. Veeraraghavan, D. Reddy, and R. Raskar, "Coded strobing photography: Compressive sensing of high speed periodic videos," *IEEE Transactions on Pattern Analysis and Machine Intelligence*, vol. 33, no. 4, pp. 671–686, 2010.

[15] A. Al-Kinani, C.-X. Wang, L. Zhou, and W. Zhang, "Optical wireless communication channel measurements and models," *IEEE Communications Surveys and Tutorials*, pp. 1939–1962, 2018.

[16] H. Henniger and O. Wilfert, "An Introduction to Free-space Optical Communications." *Radioengineering*, vol. 19, no. 2, 2010.

[17] C. Tebruegge, A. Memedi, and F. Dressler, "Empirical Characterization of the NLOS Component for Vehicular Visible Light Communication," in *IEEE VNC 2019*. Los Angeles, CA: IEEE, Dec. 2019.

[18] M. Nabeel, B. Bloessl, and F. Dressler, "Efficient Receive Diversity in Distributed Sensor Networks using Selective Sample Forwarding," *IEEE Transactions on Green Communications and Networking*, vol. 2, no. 2, pp. 336–345, Jun. 2018.